ACTA IMEKO
ISSN: 2221-870X
December 2024, Volume 13, Number 4, 1 - 6

Exploring the operational limits of a bolometric camera for thermoelastic stress measurements using a photonic reference camera

Giulio Tribbiani[1], Tiberio Truffarelli[2], Tommaso Zara[1], Roberto Marsili[1], Antonella Gaspari[3], Laura Fabbiano[3], Gianluca Rossi[2]

[1] *CISA G.Colombo, Università degli Studi di Padova, via Venezia 15, 35131 Padova, Italia*
[2] *Dipartimento di Ingegneria, Università degli Studi di Perugia, Via G. Duranti 93, 06125 Perugia, Italia*
[3] *DMMM, Politecnico di Bari, Via Orabona 4, 70126 Bari, Italia*

ABSTRACT
Image analysis-based measurement techniques are gaining popularity thanks to their ability of measuring different kinds of mechanical fields without interfering with the measurand. Thermoelastic Stress Analysis is a full field, non-contact technique that uses IR images and the principle of thermoelasticity to measure stress distributions. The low amplitude of the temperature variations and the high frequency excitations required, make it mandatory to use fast and expensive IR imaging systems. Using systems based on micro-bolometers instead of photonic sensor, could significantly reduce the cost of the instrumentation. The aim of this study is to understand how to tune the acquisition parameters of a bolometric thermal camera (i.e., the length of the thermal video) and set the right excitation frequency, to match the stress measurement obtained using a state of art photonic thermal camera. The stress concentration around the hole of a PVC sample was used to quantify the difference between the measurement results obtained by the two IR systems. The results showed how having more frames allowed to obtain more detailed maps of stress distribution and to reduce the gap between the bolometric camera and the reference one. The gap increased when the sample was tested with a frequency near the limit set by Nyquist's theorem.

Section: RESEARCH PAPER

Keywords: Thermoelasticity; image analysis; thermal imaging; non-contact stress measurement

Citation: G. Tribbiani, T. Truffarelli, T. Zara, R. Marsili, A. Gaspari, L. Fabbiano, G. Rossi, Exploring the operational limits of a bolometric camera for thermoelastic stress measurements using a photonic reference camera, Acta IMEKO, vol. 13 (2024) no. 4, pp. 1-6. DOI: 10.21014/actaimeko.v13i4.1759

Section Editor: Andrea Scorza, Università degli Studi Roma Tre, Italy

Received January 26, 2024; **In final form** May 28, 2024; **Published** December 2024

Corresponding author: Giulio Tribbiani, e-mail: giulio.tribbiani@phd.unipd.it

1. INTRODUCTION

Traditional measurement methods often encounter issue when applied to on-line monitoring of mechanical components, where accessibility and potential damage to the measurand itself become significant concerns. In response to these challenges, non-contact measurement techniques have emerged as a revolutionary approach, offering noteworthy advantages in terms of adaptability in the context of assembled systems, other than being capable of providing full-field results.

Thermoelastic Stress Analysis (TSA) [1], [2] is a well-known non-contact, full field measurement technique, used to measure mechanical stress fields on the surface of a component [3], [4]. Being able to measure stress distributions is extremely important to determine the regions where failures are more likely to occur [5], [6], [7]. Next to TSA, Digital Image Correlation (DIC) is the other main technique based on image analysis used to measure deformation fields. Both require a surface preparation of the specimen. DIC needs a high-contrast, random pattern that is essential to conduct image correlation and whose density influences the spatial resolution of the results. On the other hand, TSA, using the thermoelastic effect [8], [9] as its main working principle, generally only requires a high emissivity coating of the specimen. Despite many advantages, TSA must cope with many issues. First, to obtain a quantitative stress distribution it is necessary to reach the condition of pseudo-adiabaticity: the exciting frequency has to be high enough so that there are no heat exchanges inside the sample or between the sample and the surrounding environment. In addition, the amplitude of the temperature variation related to stress is extremely low, typically

of the same order of magnitude as measurement noise. To perform TSA it then becomes fundamental to use sophisticated and expensive IR imaging systems.

As a matter of fact, TSA gained popularity after the advent of Focal Plane Array (FPA) [10] thermal cameras, that allow to perform a full frame measurement without having to raster-scan the measurand, as with Stress Pattern Analysis by Thermal Emission (SPATE) [11] instrumentation. Using arrays of bolometric sensors [12], [13] allowed for a significant reduction in the time needed to observe the phenomenon. Although, the major step forward occurred with the arrival of photonic thermal sensors. The difference between the two lies in their working principle, affecting their ability to acquire images at different frame rates [14]. While a bolometer works as first order (e.g., a thermometer), the photonic one acts as an instrument of order zero. This means that, if it necessary to wait an appropriate amount of time (i.e., the Time Constant) for the bolometric sensor to reach the thermal equilibrium with the measurand, a photonic sensor [15], [16] produces a number of electron charges proportional to the number of incident photons in a time interval (i.e., the Integration Time). While the Integration Time can be varied and adjusted by the user, the Time Constant remains fixed and depends only on how the sensor was produced. Typically, photonic sensors can acquire more than time times faster than bolometric ones, though being much more expensive. The high cost of these kinds of thermal cameras, despite making the technique very efficient, is problematic for the take-up of TSA itself, especially in applications outside the laboratory.

Counter intuitively, a step back to micro-bolometric IR cameras could be a solution to the cost issue, but some directions of use have to be respected. In 2013 Rajic et al [17] underlined how bolometric cameras, far less expensive and more practical than photonic ones, require some corrections both in the phase and amplitude domain. In 2014, Rajic [18] further researched the difference between the bolometric and photonics IR systems, finding a significant dependency between the Signal to Noise (S/N) of the sensor and the number of the acquired loading cycles. It was found that more loading cycles meant an improvement for both sensors: while for a lower number of cycles the photonic sensor outperformed the bolometric one, the trend inverted for high numbers of cycles. The photonic sensor in fact briefly reached a performance plateau, with the bolometric keeping reducing its S/N ratio.

These results were further demonstrated in 2020 by Pitarresi [19], who defined signal processing procedures to recognise, quantify and correct errors due to spectral leakage and loss of streamed frame.

In this study a bolometric thermal camera (FLIR T1020) was used to measure the stress distribution over a PVC sample, exploring how the loading excitation frequency and the number of acquired frames affect the result. As a reference, a state of art photonic camera was used (FLIR A6751SC). While the studies found in literature are mostly focused on performing a pointwise comparison between this two thermal cameras, our work aims on expanding this approach, evaluating quantitatively the bolometric limitations over the measurement of a stress distribution, rather than on a single point. Hence, the Stress Concentration Factor (SCF) was chosen as the metric used to quantify the difference between the measurements obtained by the bolometric and photonic systems. As a matter of facts, the main applications of TSA are in measuring stress distributions in mechanical components, rather than measuring the stress state in a single location.

The paper is structured as follows: in Section 2 the fundamentals on thermoelasticity and on Lock-In signal processing are provided; in Section 3 the test protocol and the procedure used to realize the sample are explained; Section 4 is dedicated to the results and discussions.

2. FUNDAMENTALS OF THERMOELASTICITY

The analysis of the thermal images of a specimen subjected to a variable load can give useful information about its stress state if we consider that the deformations involved in the process cause temperature variations. The basic principle is well-known in gases for which even small variations in its volume, cause significant variations in temperature. The same is valid even for solid bodies, even though for them the variations in their temperature after deformation might be less evident. The correlation between the stress and temperature fields was studied by Lord Kelvin, who stated the thermoelasticity phenomenon for an isotropic linear elastic material subjected to adiabatic heat exchange, expressed by the equation:

$$\Delta T = -\frac{\alpha T_0}{\rho C_\mathrm{p}} \Delta I(\sigma) \tag{1}$$

where:

T_0 - absolute temperature of the tested body

α - thermal expansion coefficient

ρ - density

C_p - specific heat capacity at constant temperature

$\Delta I(\sigma)$ - first invariant of Cauchy's stress tensor.

Equation 1 can be considered value in the hypothesis of a negligible variation of the Young's Modulus with temperature [20]. Being the sample analysed in this study made of PVC, the temperature fluctuation is low enough to consider this hypothesis verified.

The amplitude of ΔT caused by the thermoelastic effect is extremely low: Boulanger et al [21] demonstrated that for a dual phase steel (DP60), the amplitude of the temperature variation in response to a sinusoidal tension variation $\Delta\sigma$ of 360 MPa at 1 Hz, is lower than 0.2 K.

If the heat exchange with the surrounding environment and inside the body itself is then considered, the phenomenon becomes transitory. For example, if we consider the pure bending of a simple beam, it is well known that the resulting stress state has a bi-triangular asymmetric behaviour around the neutral axis reaching the same maximum values at the top and bottom surfaces. Therefore, an equal-shaped thermal gradient arises between the opposite surfaces causing heat fluxes toward the surrounding environment and between the surfaces themselves, dissipating the temperature variation initially produced by the load.

Then, to measure the stress field in a deformed specimen, it is necessary to apply cyclic loading with frequencies depending on its material and surface-to-volume ratio. To achieve the condition of pseudo-adiabaticity and apply Kelvin's equation, a wide range of frequencies are generally tested to find the one apt to neglect the heat exchanges and to measure the ΔT corresponding to the stress state of the body.

Further, particular signal processing techniques are necessary to highlight only those contributions of the measured temperature signals related to stress. Unfortunately, that information has typically the same order of magnitude as the measurement noise.

2.1. Lock-In Signal Processing

This signal processing techniques [22], used to isolate only component of the signal at specific frequencies, needs the a priori knowledge of the frequency of the applied cyclic load to be applied. Using a dedicated sensor, (load cell, accelerometer, or displacement device), the reference $R(t)$ loading signal can be acquired, from which two square waves with the same frequency of $R(t)$ are extracted but with different phases, one called $F(t)$, in phase with the original signal, the other, $G(t)$, shifted by 90° to $R(t)$.

$$F(t) = Square(\omega\, t) \tag{2}$$

$$G(t) = Square(\omega\, t\, + \pi/2) \tag{3}$$

The signal coming from the thermal camera $S(t)$ can be considered as follows:

$$S(t) = \Delta T \sin(\omega\, t\, +\, \theta)\, +\, \chi \tag{4}$$

Being the quantities θ and χ in Equation 4 respectively the phase shifting between the temperature variation and the load applied and the measurement noise, supposed Gaussian, hence a zero-mean signal. The Lock-In Amplifier (LIA) then multiplies the signal in Equation 4 by the signals in Equation 2. To eliminate the effects of χ, a low pass filter is applied which is equivalent to average the signal over the acquisition period. The same operations are repeated, multiplying Equation 4 by Equation 3 and filtering. The results of the LIA processing are respectively the quantities I_x and I_y:

$$I_x = \Delta T \sin(\theta) \tag{5}$$

$$I_y = \Delta T \cos(\theta) \tag{6}$$

Equation 5 and Equation 6 denote the imaginary and real part of a complex number I, who has its magnitude and phase

$$I = I_x + \mathrm{j}\, I_y \tag{7}$$

$$Magnitude\, = \sqrt{(I_x^2 + I_y^2)} \tag{8}$$

$$Phase\, = \arctan\left(\frac{I_y}{I_x}\right). \tag{9}$$

The magnitude is indicative of the amplitude of the temperature variation ΔT due to the deformation of the sample, while the phase gives the sign of the deformation, hence indicating if a specific part of the body is stretching or compressing.

In this study a Digital Lock-In Amplifier was used, meaning that no other reference sensor was installed. The $R(t)$ was reconstructed as a sinusoidal thermal signal with the same frequency as the excitation.

2.2. Stress Concentration Factor (SCF)

The Stress Concentration Factor (SCF) (not to be confused with the one used for determining the tensile state of notched samples) is the metric defined to compare the stress state measured with the bolometric camera, to the one obtained using the photonic one.

Taking the ΔT map, obtained by processing the signal as explained in Section 2.1, it is possible to find the temperature variation profile along different interrogation lines. The attention is focused on the profile along the line of pixel that crosses the centre of the hole, as shown in Figure 1.

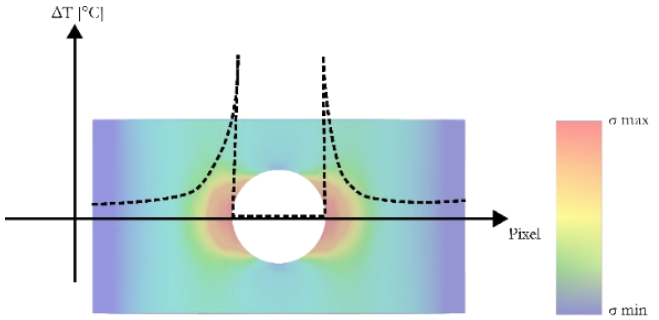

Figure 1. In the background, the expected stress distribution. Superimposed, the temperature profile (dotted line) over the pixel of the horizontal interrogation at the centre of the hole.

Using Equation 1, it is possible to obtain the maximum and mean value of stress on the profile. The maximum temperatures locate the edges of the hole in the temperature profile. The mean value of temperature is used to compute the ratio, because considered more significant than the minimum value, being less affected by noise. The SCF is calculated by computing the ratio between the two values found:

$$\begin{aligned} SCF &= \frac{\sigma_{\mathrm{Max}}}{\sigma_{\mathrm{mean}}} \\ &= -\,\Delta T_{\mathrm{Max}} \frac{T_0\, \alpha}{\rho\, C_p} \cdot \left(-\frac{1}{\Delta T_{\mathrm{mean}}}\, \frac{\rho\, C_p}{T_0\, \alpha}\right) \\ &= \frac{\Delta T_{\mathrm{Max}}}{\Delta T_{\mathrm{mean}}}. \end{aligned} \tag{10}$$

Equation 10 shows that the ratio between stresses equals the ration between temperature variations; it then becomes irrelevant to know the thermoelastic coefficient of PVC.

3. MATERIAL AND METHODS

3.1. Test Sample

A 200 × 30 mm PVC sheet was realized, with a 10 mm hole in the centre, used to mount the sample onto the shaker. To lower the resonant frequency and amplify the displacement of the tested specimen, other two 8 mm holes were drilled at the ends of sample, used to place two masses on it, each one of 27 g.

To avoid an alteration of the stress state around the central hole, the sample-shaker connection was realized with a cylindrical rubber fixation, used to eliminate the contact between the screw and the surface of the sample. When the bolt was tightened, the fixture deformed and generated a radial pressure on the lateral surface of the hole, securing the sample onto the shaker. In Figure 2 and Figure 3, representations of the sample and its connection are shown.

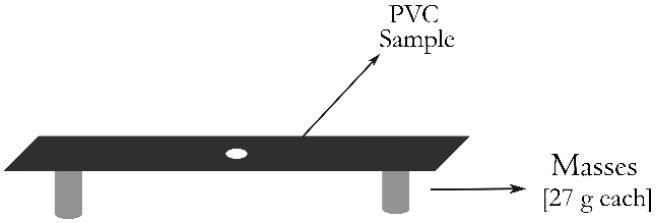

Figure 2. Position of the two masses at the ends of the specimen.

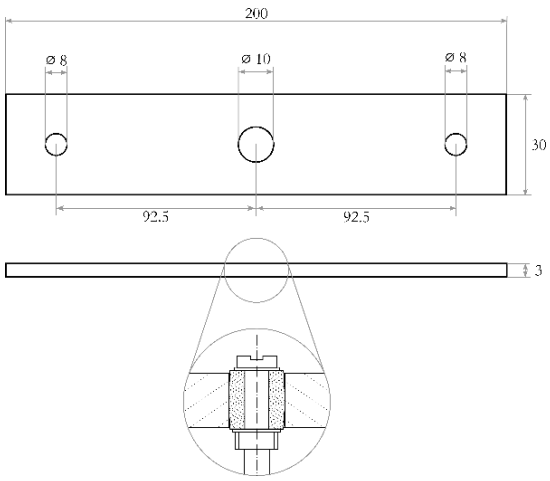

Figure 3. Design of the specimen and the locking system. Dimensions in millimetres. A focus on the detail of the connection is shown. The rubber fixation (represented with a rhombic hatching pattern) is compressed between the flat washers, tightened by the bolt.

3.2. Test Protocol

The length of the thermal video and the excitation frequency of the specimen were considered the main impact factors on the ability of the bolometric thermal camera to detect the stress state using the thermoelastic principle described in Section 2. The FLIR T1020 with a 34 mm lens was the bolometric thermal camera used in this study. The FLIR A6751SC with a 50 mm lens was the photonic camera used as a reference.

The photonic and bolometric camera acquired the thermal video at 60 Hz and 30 Hz, respectively.

The A6751SC produced sharper images than the T1020, despite having a lower resolution sensor: 640 × 512 pixels for the first one and 1024 × 758 pixels for the second one. To account for the geometrical resolution of the cameras (i.e., the millimetres covered by a single pixel), the ratio were calculated and resulted: 1.03 mm/pixel for the bolometric camera and 1.31 mm/pixel for the photonic camera. As there is no significant difference in these geometrical resolutions, the reason to the gap in sharpness mainly lies in the higher S/N ratio of the photonic sensor rather than the bolometric one, 10^{10} and 10^{8} [23], respectively. The influence of the viewing angle is negligible [24].

In Table 1, a brief comparison between the characteristics of the two cameras is shown.

A Brüel & Kjær V201-M4-CE electrodynamic shaker was used to excite the sample with fixed frequency sine waves generated with a HAMEG HM8030-6. A representation of the bench is shown in Figure 4.

This configuration eliminates the need to apply any motion compensation algorithm [25], [26] to the video. The issue is that rigid motions of the sample create ΔT localized at its edges. These unwanted concentrations are not related to stress and can

Table 1. Focus on the characteristics of the two thermal cameras.

Specification	A6751SC	T1020
Sensor Dimensions	640 × 512 pixels	1024 × 758 pixels
Max fps (at full frame)	125 fps	30 fps
S/N Ratio	10^{10}	10^{8}
NETD	< 20 mK	< 20 mK
Cost	~ 75 000 €	~ 25 000 €

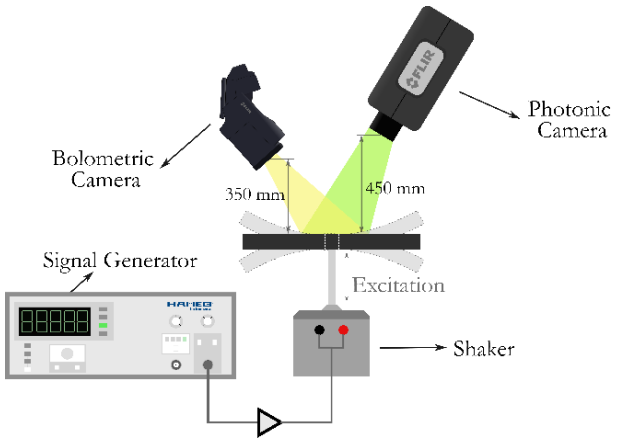

Figure 4. Representation of the test bench with the photonic (A6751SC) and bolometric (T1020) facing the sample on the electrodynamic shaker. The cameras are placed at different distances, to ensure a similar geometrical resolution, despite the different focal length.

lead to misleading results. The bending motion of the ends of the sample has also components non-orthogonal to the plane of the camera. These components are the one responsible of such unwanted ΔT concentrations. However, the ROI (Region Of Interest) is at the centre of the rectangular plate, where deformation is located, but no bending happens. The only displacement of this part of the sample is orthogonal to the camera, irrelevant to the edge effect.

The sample is tested with a sinusoidal displacement at 3 different frequencies: 5, 10 and 15 Hz. In this way, the bolometric camera is tested up to the frequency limit imposed by Nyquist's condition. For each frequency, 3 videos are captured, with a length respectively of 10, 20 and 30 s. The tests at 10 Hz are repeated a total of 3 times for each video length. The standard deviation is then calculated for the bolometric and photonic SCFs. These standard deviations are extended for the other excitation frequencies.

4. RESULTS AND DISCUSSIONS

The analysis shows the impact of the loading frequency and the length of the video on the TSA maps obtained using the T1020 in comparison with the A6751SC.

In Figure 5, it is possible to focus the attention on the effect of the length of the video, fixing the excitation frequency at 10 Hz. The results show how longer videos allow to obtain ΔT maps with a significantly improved S/N ratio. The explanation is to be attributed to the LIA signal processing. The LIA acts as an integrator, hence it computes the average between all the frames of the thermal video. Thus, having more frames (i.e., longer

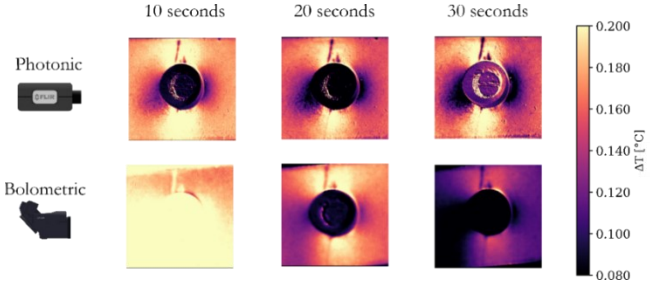

Figure 5. Effect of the length of the video on the ΔT maps obtained from thermal images acquired with both the photonic (A6751SC) and bolometric (T1020). Excitation frequency was 10 Hz for all cases.

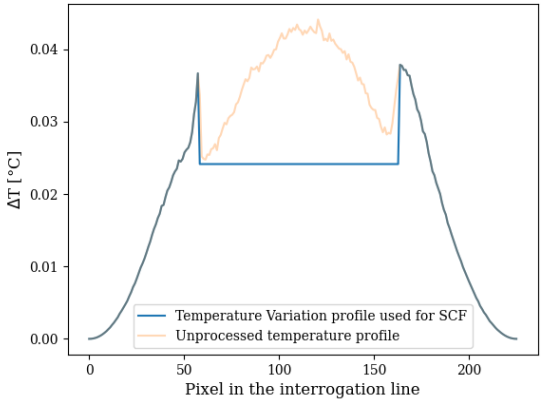

Figure 6. Resulting Δ*T* profile obtained using the T1020 (video length: 30 s - loading frequency: 10 Hz).

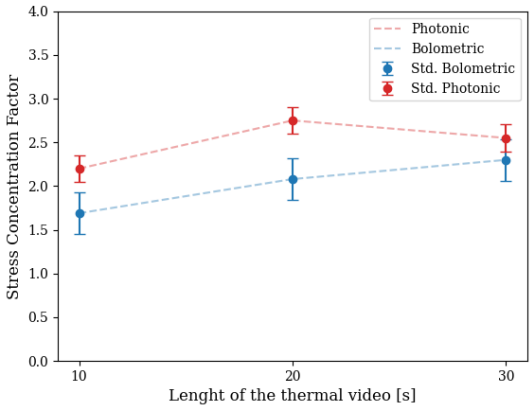

Figure 8. The highest difference between the mean SCF measured with the bolometric IR camera (in red) and the photonic one (in blue) was found with the 20 s long thermal videos, where the results obtained with the photonic camera did no longer improve by averaging more frames.

videos), means having more data to average. While this improvement can also be seen in the results from the photonic camera, having many frames becomes fundamental when using a bolometric camera.

For each Δ*T* map obtained via LIA, it is possible to determine the SCF using Equation 10. The area of focus are the pixels around the hole. Figure 6 shows how the temperature variation profile was processed to remove unwanted information from the pixel containing the screw. Ideally, the Δ*T* profile should have the trend shown in Figure 1. Hence, once located the maximum Δ*T*s at both edges of the hole, the values in between the two maxima were replaced with the mean of the signal. The procedure is repeated for each acquisition of both cameras.

A total of 18 SCF were obtained: two for each of the 9 test configurations. Being the A6751SC the reference, it was calculated the difference between the bolometric and photonic SCF for each configuration.

In Figure 7 the SCF differences are shown. The results are given as percentages, as each difference was then normalized over the maximum SCF (i.e., the higher one between all the experimental configurations). In this way, the comparison between the acquisition set-up is more effective.

As it was expected, processing longer thermal videos allowed to reduce the gap between the concentration factors obtained by the two systems. A significant drop in performance was noticed at 15 Hz, being the higher frequency limit set by Nyquist's theorem [27], [28]. In facts, the T1020 is only capable of

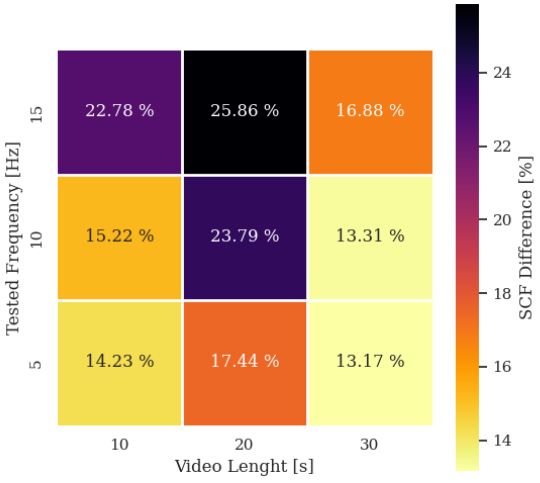

Figure 7. Comparison heatmap between the mean SCF differences, obtained by processing the video acquired by the two thermal cameras.

acquiring thermal video only at 30 fps, a sampling rate only twice bigger than the frequency excitation.

Another result worth notice was that the higher SCF difference was found at the 20 s long videos, not at the 10 s long ones, as was expected. The explanation of this behaviour is visible in Figure 8, where, fixing the excitation frequency at 10 Hz, the SCF of the two cameras were plotted against the length of the video. The trends show that working with longer videos also improves the performance of the photonic camera. Nevertheless, the photonic SCF reached a plateau after the 20 s long video, meaning that the number of frames was sufficient so that further increasing the length of the video did not changed significantly the average value. On the other hand, the behaviour of the SCF for the bolometric camera is much more linear. Taken together, these effects cause the highest SCF difference to be shifted from where it was expected.

5. CONCLUSIONS

Reducing the instrumentation cost for TSA measurements is fundamental to allow a further spread of this full-field, non-contact technique. Working with bolometric cameras instead of photonic ones could be a major step forward in this direction.

This study focuses on exploring how setting the appropriate acquisition parameters and excitation conditions to thin the gap between the results obtained by a bolometric and a photonic thermal acquisition system.

The length of the thermal video resulted as one of the key factors when using a bolometric IR camera. Because of the signal processing techniques used to obtain the stress state of a sample, having more frames means having more data for the LIA to average, resulting in less noisy Δ*T* maps. Setting the proper acquisition length allowed to reduce the difference between the system from 23 % down to 13 %, working with the same excitation frequency.

Another key aspect to take into account is the frequency of the excitation signal with respect to the frame rate of the IR camera used. Working with signals with frequency components right at the limit set by Nyquist theorem, strongly effects the quality of the measurement, increasing the gap between the bolometric and photonic results, obtained adopting the LIA signal processing. Considering the tests with 30 s long acquisition, exciting the sample at the Nyquist limit produced a

difference between the bolometric and photonic system of 17 %, reduced to 13 % by using cyclic loads at 5 Hz and 10 Hz.

Future studies will be mainly focused on determine if, with a proper video length and test condition, this upper limit can be pushed beyond Nyquist theorem, acquiring aliased signals with a bolometric thermal camera.

ACKNOWLEDGEMENT

The searches mentioned in this paper are funded by the European Union LIFE Program, Green Casting LIFE Project (LIFE21-ENV-FI-Project101074439). Views and opinions expressed are however those of the author(s) only and do not necessarily reflect those of the European Union or CINEA. Neither the European Union nor the granting authority can be held responsible for them.

REFERENCES

[1] G. Pitarresi, E. A. Patterson, A review of the general theory of thermoelastic stress analysis, The Journal of Strain Analysis for Engineering Design 38 (2003) no. 5, pp. 405–417. DOI: 10.1243/03093240360713469

[2] R. J. Greene, E. A. Patterson, R. E. Rowlands, Thermoelastic Stress Analysis, Springer handbook of experimental solid mechanics (2008), pp. 743-768. DOI: 10.1007/978-0-387-30877-7_26

[3] L. Capponi, T. Tocci, M. D'Imperio, S. H. J. Abidi, M. Scaccia, F. Cannella, R. Marsili, G. Rossi, Thermoelasticity and ArUco marker-based model validation of polymer structure: application to the San Giorgio's bridge inspection robot, Acta IMEKO 10 (2021) no. 4, pp. 177–184. DOI: 10.21014/acta_imeko.v10i4.1148

[4] L. Capponi, J. Slavič, G. Rossi, M. Boltežar, Thermoelasticity-based modal damage identification, International Journal of Fatigue 137 (2020), p. 105661. DOI: 10.1016/j.ijfatigue.2020.105661

[5] A. Quattrocchi, D. Alizzio, L. Capponi, T. Tocci, R. Marsili (+ 9 more authors), Measurement of the structural behaviour of a 3D airless wheel prototype by means of optical non-contact techniques, Acta Imeko 11 (2022) no. 3, pp. 1–8. DOI: 10.21014/acta_imeko.v11i3.1268

[6] R. Montanini, G. Rossi, A. Quattrocchi, D. Alizzio, L. Capponi, R. Marsili, A. Di Giacomo, T. Tocci, Structural characterization of complex lattice parts by means of optical non-contact measurements, Proc. of the 2020 IEEE Int. Instrumentation and Measurement Technology Conf. (I2MTC), IEEE, pp. 1–6. DOI: 10.1109/I2MTC43012.2020.9128771

[7] G. Allevi, L. Capponi, P. Castellini, P. Chiariotti, F. Docchio, F. Freni, R. Marsili, M. Martarelli (+ 7 more authors), Investigating additive manufactured lattice structures: a multi-instrument approach, IEEE Transactions on Instrumentation and Measurements 69 (2019) no. 5, pp. 2459–2467. DOI: 10.1109/TIM.2019.2959293

[8] R. B. Hetnarski, J. Ignaczak, Generalized thermoelasticity, Journal of Thermal Stresses 22 (1999), no. 4–5, pp. 451–476. DOI: 10.1080/014957399280832

[9] A. E. Green, K. A. Lindsay, Thermoelasticity, Journal of Elasticity 2 (1972) no. 1, pp. 1–7: DOI: 10.1007/BF00045689/METRICS

[10] A. Rogalski, Progress in focal plane array technologies, Progress in Quantum Electronics 36 (2012), pp. 342-473. DOI: 10.1016/j.pquantelec.2012.07.001

[11] D. S. Mountain, J. M. B. Webber, Stress pattern analysis by thermal emission (SPATE), Proc. of the 4th European Electro-Optics Conference (1979).

[12] H. Jakobsen, F. Niklaus, C. Vieider, MEMS/MOEMS technologies and applications 3 (2008). DOI: 10.1117/12.755128

[13] Y. Tanaka, A. Tanaka, K. Iida, T. Sasaki, S. Tohyama, A. Ajisawa, K. Akihiro, K. Seiji (+ 6 more authors), Performance of 320x240 uncooled bolometer-type infrared focal plane arrays, Infrared Technology and Applications (2003), pp. 414-424. DOI: 10.1117/12.499259

[14] R. Gade, T. B. Moeslund, Machine vision and applications 25 (2014), pp. 245-262. DOI: 10.1007/s00138-013-0570-5

[15] S. Roux, P. Barritault, O. Lartigue, O., L. Cerutti, E. Tournié, B. Gérard, A. Grisard, Mid-infrared characterization of refractive indices and propagation losses in GaSb/AlXGa1− XAsSb waveguides, Applied Physics Letters, 107 (2015). DOI: 10.1063/1.4934702/28700

[16] S. B. Venkataraman, B. Raj, Performance parameters for thermal imaging systems, Insight: Non-Destructive Testing and Condition Monitoring 45 (2003) no. 8, pp. 531–535. DOI: 10.1784/INSI.45.8.531.52914

[17] N. Rajic, D. Rowlands, Thermoelastic stress analysis with a compact low-cost microbolometer system, Quantitative infrared thermography journal 10 (2013), pp. 135-158. DOI: 10.1080/17686733.2013.800688

[18] N. Rajic, N. Street, A performance comparison between cooled and uncooled infrared detectors for thermoelastic stress analysis, Quantitative InfraRed Thermography Journal 11 (2014), pp. 207-221. DOI: 10.1080/17686733.2014.962835

[19] G. Pitarresi, R. Cappello, G. Catalanotti, Quantitative thermoelastic stress analysis by means of low-cost setups, Optics and Lasers in Engineering (2020), p. 106158. DOI: 10.1016/j.optlaseng.2020.106158

[20] N. Merah, M. Irfan-ul-Haq, Z. Khan, Temperature and weld-line effects on mechanical properties of CPVC, Journal of Materials Processing Technology 142 (2003), pp. 247-255. DOI: 10.1016/S0924-0136(03)00567-3

[21] T. Boulanger, A. Chrysochoos, C. Mabru, A. Galtier, Calorimetric analysis of dissipative and thermoelastic effects associated with the fatigue behavior of steels, International Journal of Fatigue 26 (2004), pp. 221–229. DOI: 10.1016/S0142-1123(03)00171-3

[22] J. Gaspar, S. F. Chen, A. Gordillo, M. Hepp, P. Ferreyra, C. Marqués, Digital lock in amplifier: study, design and development with a digital signal processor, Microprocessors and Microsystems, 28 (2004), pp. 157-162. DOI: 10.1016/j.micpro.2003.12.002

[23] M. J. Riedl, Optical Design Fundamentals for Infrared Systems, Second Edition (2009). DOI: 10.1117/3.412729

[24] M. Ball, H. Pinkerton, Factors affecting the accuracy of thermal imaging cameras in volcanology, Journal of Geophysical Research: Solid Earth 111 (2006), p. 11203. DOI: 10.1029/2005JB003829

[25] T. Tocci, L. Capponi, R. Marsili, G. Rossi, Optical-flow-based motion compensation algorithm in thermoelastic stress analysis using single-infrared video, Acta IMEKO 10 (2021), no. 4, pp. 169–176. DOI: 10.21014/acta_imeko.v10i4.1147

[26] G. Tribbiani, T. Zara, T. Truffarelli, L. Capponi, Fiducial marker and blob detection-based motion compensation algorithm for Thermoelastic Stress Analysis measurements, Journal of Physics: Conf. Series 2698 (2024) no. 1, p. 12001. DOI: 10.1088/1742-6596/2698/1/012001

[27] H. J. Landau, Sampling, data transmission, and the Nyquist rate, Proc. of the IEEE (1967), pp. 1701-1706. DOI: 10.1109/PROC.1967.5962

[28] A. J. Jerri, The Shannon Sampling Theorem - Its Various Extensions and Applications: A Tutorial Review, Proceedings of the IEEE (1977), pp. 1565–1596. DOI: 10.1109/proc.1977.10771